molecules

MDPI

Article

Small Molecule Drugs That Inhibit Phagocytosis

Melika Loriamini [1,2], Melissa M. Lewis-Bakker [3], Kayluz Frias Boligan [1], Siming Wang [3], Mairead B. Holton [1], Lakshmi P. Kotra [3,4,*] and Donald R. Branch [1,2,5,6,*]

1 Centre for Innovation, Canadian Blood Services, Toronto, ON M5G 2M1, Canada
2 Department of Laboratory Medicine and Pathobiology, University of Toronto, Toronto, ON M5S 1A8, Canada
3 Krembil Research Institute, University Health Network, Toronto, ON M5G 1L7, Canada
4 Department of Pharmaceutical Sciences, Leslie Dan Faculty of Pharmacy, University of Toronto, Toronto, ON M5S 3M2, Canada
5 Department of Medicine, University of Toronto, Toronto, ON M5S 1A8, Canada
6 Keenan Research Centre, Canadian Blood Services, Toronto, ON M5B 1W8, Canada
* Correspondence: p.kotra@utoronto.ca (L.P.K.); don.branch@utoronto.ca (D.R.B.); Tel.: +1-416-581-7602 (L.P.K.); +1-416-313-4458 (D.R.B.)

Abstract: In our initial publication on the in vitro testing of more than 200 compounds, we demonstrated that small molecules can inhibit phagocytosis. We therefore theorized that a small molecule drug discovery-based approach to the treatment of immune cytopenias (ITP, AIHA, HTR, DHTR) is feasible. Those earlier studies showed that small molecules with anti-phagocytic groups, such as the pyrazole core, are good models for producing efficacious phagocytosis inhibitors with low toxicity. We recently screened a chemical library of 80 compounds containing pyrazole/isoxazole/pyrrole core structures and found four hit molecules for further follow-up, all having the pyrazole core structure. Subsequent evaluation via MTT viability, LDH release, and apoptosis, led to the selection of two lead compounds with negligible toxicity and high efficacy. In an in vitro assay for inhibition of phagocytosis, their IC_{50} values were 2–4 μM. The rational development of these discoveries from hit to lead molecule stage, viz. independent synthesis/scale up of hit molecules, and in vivo activities in mouse models of autoimmune disease, will result in the selection of a lead compound(s) for further pre-clinical evaluation.

Keywords: immune cytopenias; phagocytosis inhibitors; drug discovery; medicinal chemistry

check for updates

Citation: Loriamini, M.; Lewis-Bakker, M.M.; Frias Boligan, K.; Wang, S.; Holton, M.B.; Kotra, L.P.; Branch, D.R. Small Molecule Drugs That Inhibit Phagocytosis. *Molecules* **2023**, *28*, 757. https://doi.org/10.3390/molecules28020757

Academic Editor: Diego Muñoz-Torrero

Received: 22 December 2022
Revised: 5 January 2023
Accepted: 7 January 2023
Published: 12 January 2023

Copyright: © 2023 by the authors. Licensee MDPI, Basel, Switzerland. This article is an open access article distributed under the terms and conditions of the Creative Commons Attribution (CC BY) license (https://creativecommons.org/licenses/by/4.0/).

1. Introduction

Immune cytopenias are conditions in which people generate antibodies against certain types of hematopoietic cells in their blood [1–3]. Cells become coated with antibodies under these circumstances and are identified by the Fcγ receptors (FcγR) on the membrane of mononuclear phagocytes. Such recognition by monocyte-macrophages results in extravascular hemolysis in the spleen and/or liver macrophages due to FcγR-mediated phagocytosis [2]. Affected individuals can face severe and sometimes even life-threatening complications due to this process [2]. Immune cytopenias have many categories [2], including (i) immune thrombocytopenia (ITP; autoimmune disease characterized by increased platelet destruction in the spleen and liver and/or decreased platelet production in the bone marrow); (ii) hemolytic disease of the fetus and newborn (HDFN; maternal hemolytic antibodies crossing the placenta); (iii) autoimmune hemolytic anemia (AIHA; phagocytosis of autoantibody-coated red blood cells); (iv) alloimmune hemolytic anemias such as hemolytic transfusion reaction (HTR; phagocytosis of donor red blood cells due to preformed hemolytic alloantibodies to the donor red cell antigens); (v) delayed hemolytic transfusion reaction (DHTR; development of hemolytic alloantibodies following transfusion); and (vi) autoimmune neutropenia (AIN) associated with autoantibodies produced against neutrophils, mainly affecting children.

The common factor of all immune cytopenias is the destruction of particular blood cells opsonized with antibodies, which requires FcγR-mediated phagocytosis. Thus, developing small molecule agents (drugs) that provides blockade of the phagocytosis would ameliorate the various immune cytopenias, and elucidation of such drugs would provide a useful clinical intervention [3,4].

The chemical synthesis and evaluation of several small molecules as potential therapeutics for ITP have been previously reported [5,6]. These heterocyclic molecules consisted of substituted pyrroles, pyrazoles, and bis-pyrazoles with S-S, C-C and C-N linkages. Evaluation of these molecules was conducted using the monocyte monolayer assay (MMA), a highly adaptable in vitro assay that can be modified to examine different aspects of antibody and Fc receptor (FcR)-mediated phagocytosis in both research and clinical settings [7,8]. Many FcRs (such as FcRI, FcRIIA, FcRIIB, FcRIIC, and FcRIIIA) are important in immunological responses and are expressed on these monocytes and macrophages. Antibody-sensitized red blood cells (RBCs) attach to and/or activate FcRs, prompting the monocyte-macrophages to phagocytose them, a mechanism the MMA uses to its advantage [7–9]. Adherent monocytes from peripheral blood mononuclear cells isolated from whole blood in mammals are used for testing, and the number of phagocytosed anti-D-opsonized red cells is visually enumerated [7]. It was demonstrated that these small molecules were capable of inhibiting phagocytosis [5,6], although robust inhibition was not observed.

In a continued effort to identify in vitro phagocytosis inhibitor(s) with high efficacy and negligible toxicity, and subsequently move to in vivo testing in animal models of immune cytopenias, molecules with additional structural modification(s) were examined. Here, in this report, are results of an in vitro screen of 80 compounds—obtained from a commercially available chemical library—leading to two compounds with negligible toxicity and high efficacy for inhibition of phagocytosis. These two molecules fulfill criteria as potential lead compounds and can be advanced to the evaluation in animal models of autoimmune cytopenias.

2. Results

2.1. Selection of Compounds for In Vitro Screening

Figure 1 shows the selection process of small molecule agents for the inhibition of phagocytosis. An in silico screen of a commercial library containing more than 13,000 compounds was conducted using physicochemical parameters. From this screen, a 5000 compound library was acquired and further narrowed to 80 compounds, using several core structural moieties of previously investigated small molecules [6]. These 80 compounds were evaluated in vitro, resulting in two lead compounds, as described in subsequent sections below.

2.2. Monocyte Monolayer Assay (MMA)

The selected 80 compounds were initially screened in an in vitro phagocytosis experiment, referred to as the monocyte monolayer assay (MMA) [7–9], at a concentration of 5 μM (Figure 2). Compounds were compared to the reference compound, intravenous immunoglobulin (IVIG) at a concentration of 1 mg/mL. Following this preliminary screen, 19 compounds that inhibited anti-D-opsonized Rh(D+) red cell phagocytosis by at least 40% were identified and chosen for further evaluation (Table 1). Phase contrast microscopy images of the MMA show phagocytosis of untreated red blood cells (RBCs) by human monocytes (Figure 3A) and the inhibition in RBCs treated with either IVIG or compounds (Figure 3B–D).

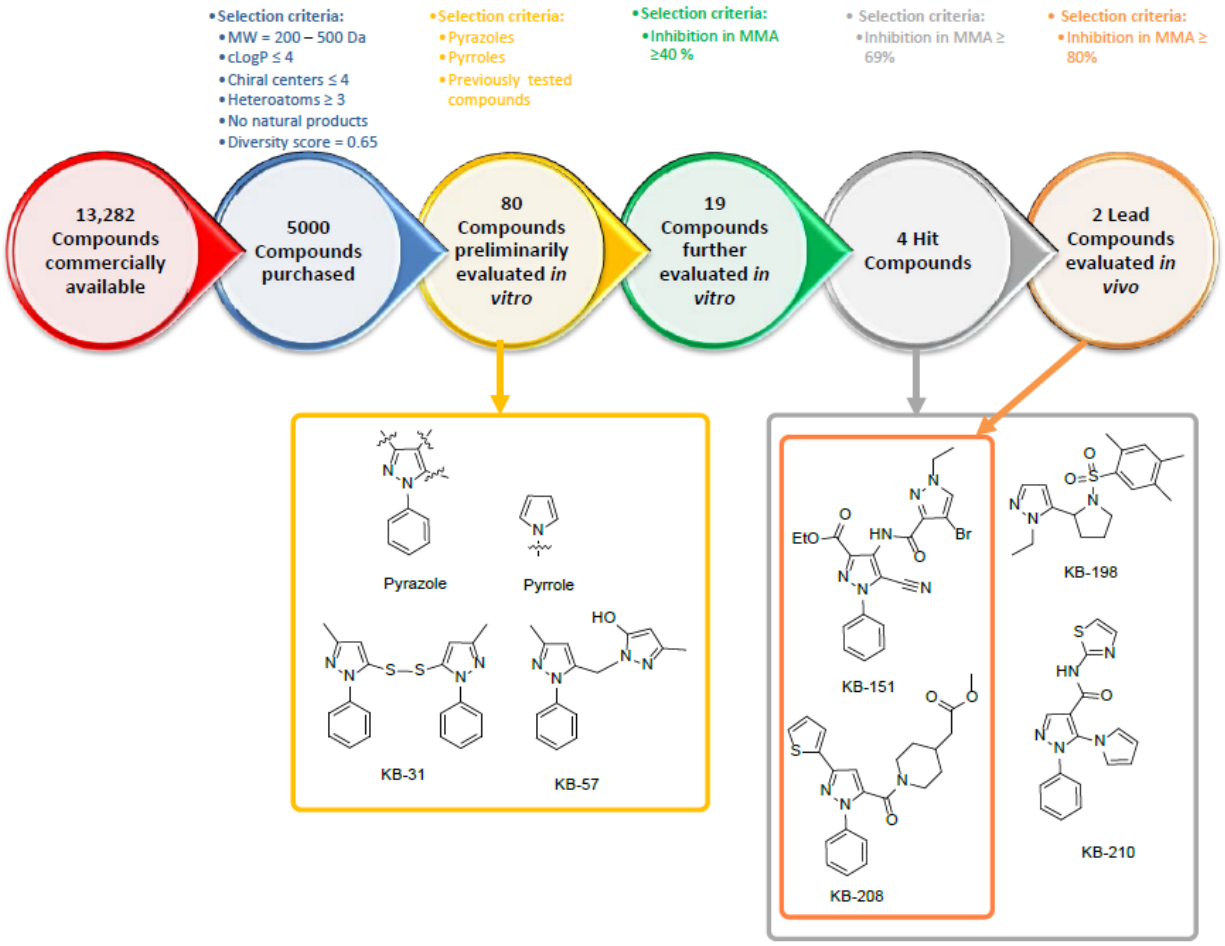


Figure 1. Selection process of compounds screened in vitro for the inhibition of phagocytosis.

Table 1. Compounds that inhibited anti-D-opsonized Rh(D+) by ≥ 40% phagocytic inhibition.

Chemical Compound	PI [1]-Average	Inhibition%
KB-151	17	80
KB-167	14	53
KB-175	15	50
KB-178	29	53
KB-179	14	53
KB-181	37	45
KB-182	28	55
KB-186	28	55
KB-189	30	52
KB-190	27	56
KB-198	9	75
KB-199	40	40
KB-205	19	47
KB-206	18	50
KB-208	7	81
KB-209	18	50
KB-210	11	69
KB-212	19	47
KB-213	13	64

[1] Phagocytosis Index (PI) $= \frac{\text{\# of phagocytic RBCs}}{\text{300 monocytes}} \times 100$.

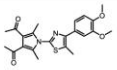
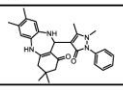
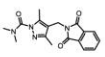
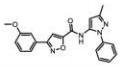
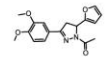
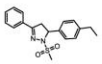
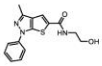
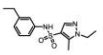
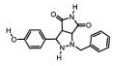
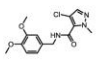
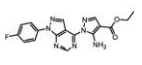
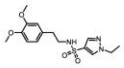
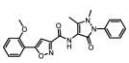
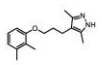
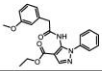
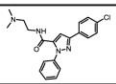
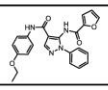
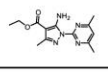
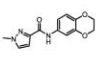
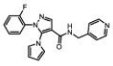
Code	Structure	Average Inhibition (%± SD)	Code	Structure	Average Inhibition (%± SD)	Code	Structure	Average Inhibition (%± SD)	Code	Structure	Average Inhibition (%± SD)
KB-132		-9± 3.47	KB-152		2 ± 8.84	KB-173		-8 ± 8.88	KB-194		39 ± 4.96
KB-133		24 ± 8.98	KB-153		8 ± 8.30	KB-174		39 ± 9.53	KB-195		25 ± 6.35
KB-134		9± 6.99	KB-154		2 ± 5.19	KB-175		50 ± 1.45	KB-196		24 ± 5.76
KB-135		18 ± 2.70	KB-155		8 ± 9.35	KB-176		-10 ± 7.06	KB-197		45 ± 4.97
KB-136		-4 ± 1.82	KB-156		2 ± 6.64	KB-177		4 ± 9.76	KB-198		75 ± 4.76
KB-137		10 ± 1.21	KB-157		3 ± 9.96	KB-178		53 ± 5.11	KB-199		40 ± 5.46
KB-138		38 ± 6.56	KB-158		0 ± 9.11	KB-179		53 ± 1.18	KB-200		31 ± 1.84
KB-139		6 ± 4.38	KB-159		15 ± 8.40	KB-180		-42 ± 8.81	KB-201		0 ± 5.41
KB-140		31 ± 7.84	KB-160		-2 ± 5.32	KB-181		-11 ± 10.27	KB-202		33 ± 2.31
KB-141		36 ± 9.37	KB-161		7 ± 8.43	KB-182		55 ± 3.65	KB-203		27 ± 2.72
KB-142		11 ± 6.51	KB-162		-37 ± 2.59	KB-183		-28 ± 9.96	KB-204		36 ± 3.60
KB-143		10 ± 6.87	KB-163		-30 ± 1.77	KB-184		7 ± 2.92	KB-205		47 ± 0.98
KB-144		33 ± 1.10	KB-164		-3 ± 9.70	KB-185		-3 ± 3.60	KB-206		50 ± 5.46
KB-145		4 ± 0.06	KB-165		33 ± 5.30	KB-186		55 ± 8.43	KB-207		14 ± 1.86
KB-146		10 ± 9.56	KB-166		17 ± 3.91	KB-187		-16 ± 9.33	KB-208		81 ± 3.43
KB-147		0 ± 3.16	KB-167		53 ± 4.18	KB-188		-26 ± 7.94	KB-209		50 ± 1.02
KB-148		28 ± 9.62	KB-168		23 ± 3.86	KB-189		52 ± 4.75	KB-210		69 ± 5.32
KB-149		0 ± 2.56	KB-169		0 ± 5.57	KB-190		56 ± 1.24	KB-211		33 ± 2.31
KB-150		24 ± 8.58	KB-170		-13 ± 4.31	KB-191		-23 ± 7.85	KB-212		47 ± 9.67
KB-151		80 ± 3.68	KB-171		7 ± 0.39	KB-192		-29 ± 9.54	KB-213		64 ± 8.74

Figure 2. Chemical structures and % inhibition (mean ± SD) in MMA of the 80 compounds preliminarily evaluated in vitro. Compounds were screened at 5 μM and compared to the reference compound, intravenous immunoglobulin (IVIG) at 1 mg/mL.

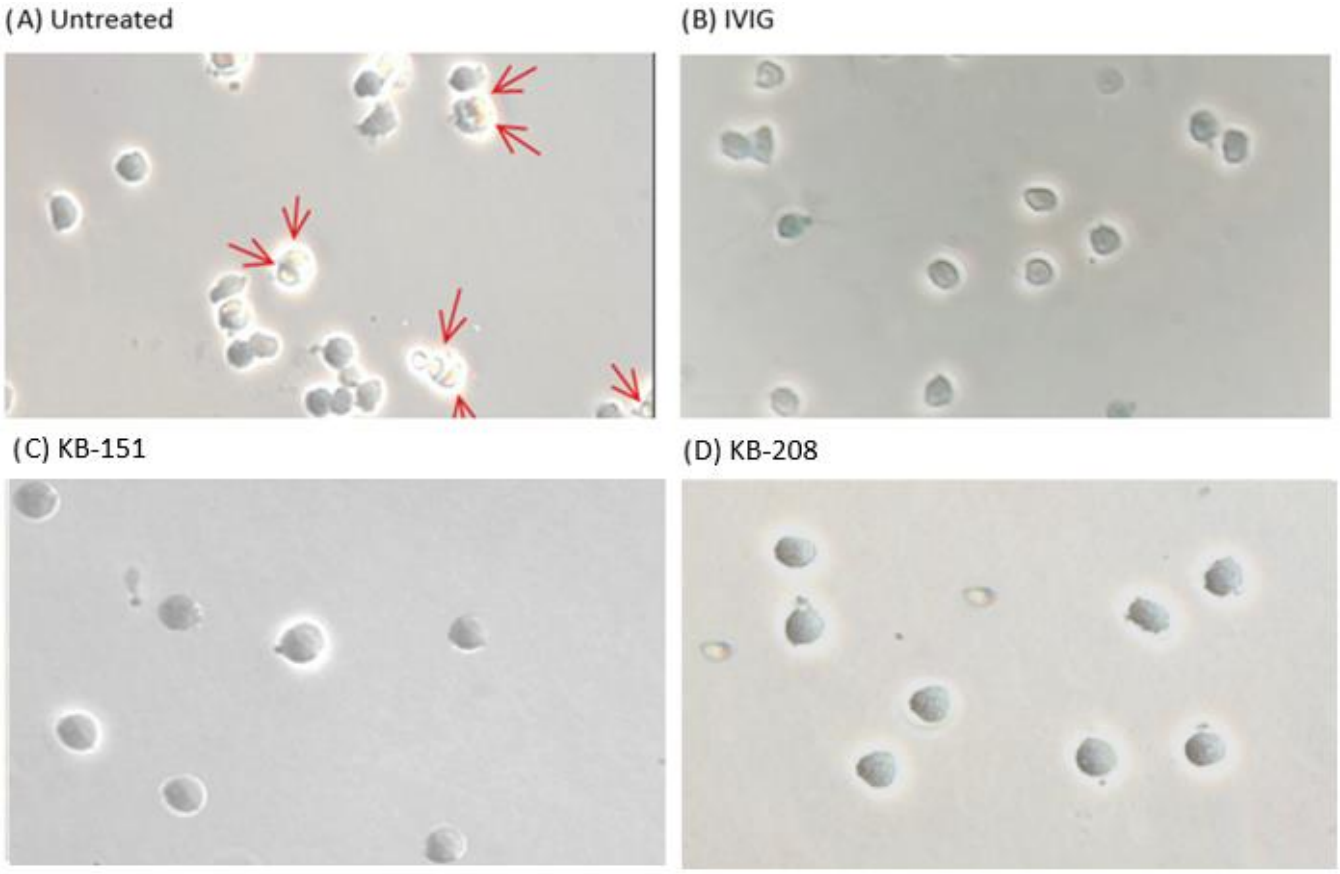


Figure 3. Phase contrast microscopy images. (**A**) Untreated human monocytes- representing monocytes phagocytosing RBCs opsonized with anti-D. Red arrows indicate RBCs that are phagocytosed (RBCs inside of monocytes). (**B**) Inhibitor control- Human monocytes treated with 1 mg/mL of IVIG. (**C**) Human monocytes treated with 100 μM KB-151. (**D**) Human monocytes treated with 100 μM KB-208.

2.3. LDH Release and MTT Assays

Additionally, these 19 compounds were tested for toxicity at a concentration of 5 μM, using an LDH release assay (Figure 4A) for a weakened cell membrane and the MTT assay for cell viability (Figure 4B). Both are colorimetric assays, but LDH relies on the release of LDH enzymes into the culture medium after cell membrane disruption [10]. As a result, the production of color suggests cytolysis. Thimerosal is a potent inhibitor of anti-Rh(D)-coated red blood cells, but does display moderate toxicity, therefore, 100 μM was used as a positive control for cell damage [11]. Compounds **KB-181**, **KB-182**, **KB-198**, **KB-199**, **KB-209**, and **KB-210** demonstrated little toxicity in these experiments compared to the control, thimerosal (100 μM), but were not significant when compared to untreated control. None of the other compounds released any LDH enzymes into the culture medium (Figure 4A).

The MTT test is a metabolic activity assay based on the enzymatic conversion of MTT in mitochondria, and color formation is an indicator of cell viability [12,13]. Thimerosal at 100 μM (**** $p \leq 0.0001$), **KB-178** (* $p < 0.05$), and **KB-182** (** $p < 0.005$) all demonstrated statistically significant changes when compared to the untreated control (tested by Kruskal–Wallis test). Other compounds showed no statistically significant changes from the untreated control (Figure 4B).

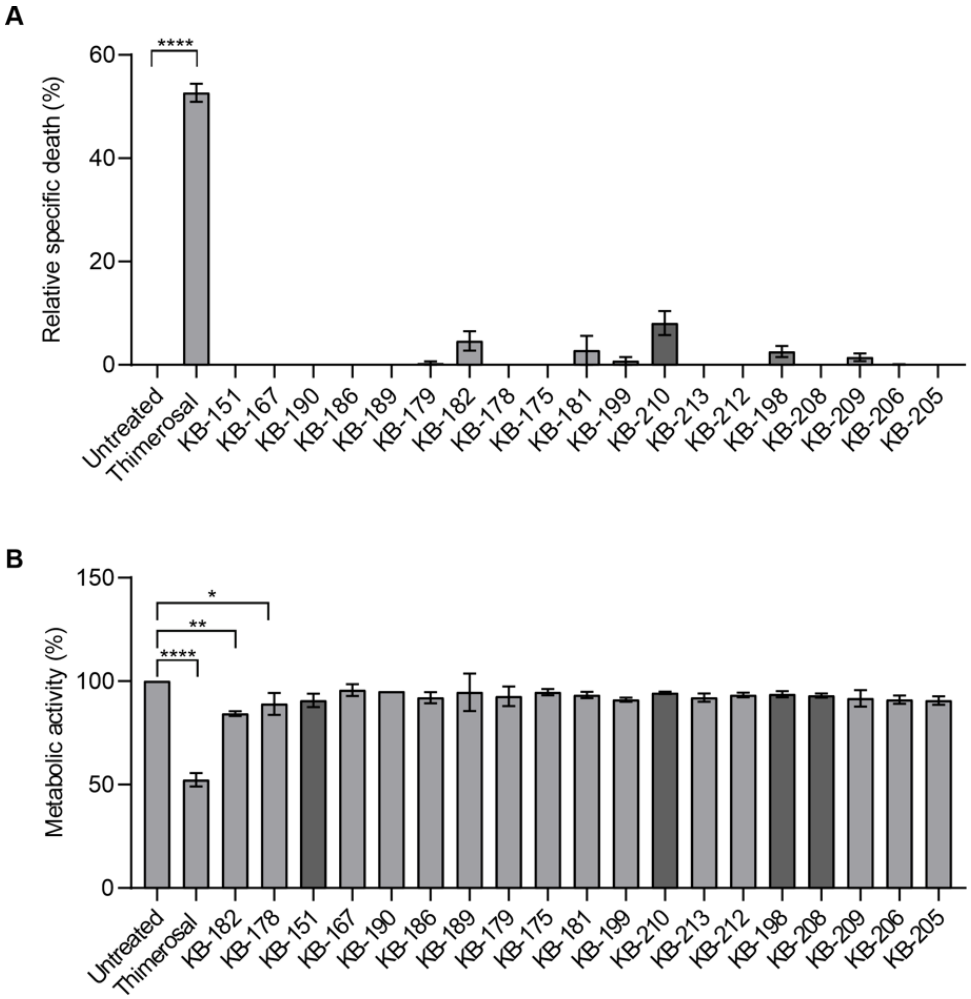


Figure 4. (**A**). LDH results: *Y*-axis shows the percentage of cell death. Thimerosal at 100 μM (**** $p \leq 0.0001$) shows a significant difference compared to untreated control. (**B**). MTT results: *Y*-axis shows the percentage of cell viability which relates to the cell metabolic activity. Thimerosal at 100 μM (**** $p \leq 0.0001$), **KB-178** (* $p < 0.05$) and **KB-182** (** $p < 0.005$) show significant differences compared to untreated control. Bars represent the mean ± SD and N = 3. The four hit compounds are shown in a darker colour.

2.4. Dose-Dependent Inhibition

For further investigation, compounds that inhibited phagocytosis by at least 65 percent in the primary screening and those that showed no toxicity in the LDH and MTT assays were selected. The selected compounds were **KB-151**, **KB-198**, **KB-208**, and **KB-210**. The dose-inhibitory responses of these four drugs were determined, and the IC_{50} values were calculated. IC_{50} values for **KB-198** and **KB-210** were more than 5 μM; IC_{50} values for **KB-151** and **KB-208** were 2.7 ± 0.8 μM and 4.2 ± 1.2 μM, respectively (Figure 5A). Ten different donors were tested with **KB-151** to determine the mean ± SD of the IC_{50}. Although similar to the original value, as expected, the value for the IC_{50} increased to 8.7 ± 9.2 μM. Similar additional testing for the IC_{50} using 10 different donors with **KB-208** revealed IC_{50} 10.1 ± 7.9 μM. Since the dose-response curves and IC_{50} values for **KB-151** and **KB-208** were the most favorable, and their MTT and LDH results revealed no significant toxicity, they were chosen for further evaluation as lead compounds. The IC_{50} values in mice PBMCs (BALB/c) and RAW 264.7 (mouse macrophage cell line) for the lead compounds (Figure 5B,C, respectively) were also calculated. The IC_{50} values for **KB-151** were 40.1 ± 13.8 μM (mouse PBMCs) and 50.7 ± 43.1 μM (RAW 264.7); IC_{50} values for **KB-208** were 59.2 ± 18.4 μM (mouse PBMCs) and 86.1 ± 71.6 μM (RAW 264.7).

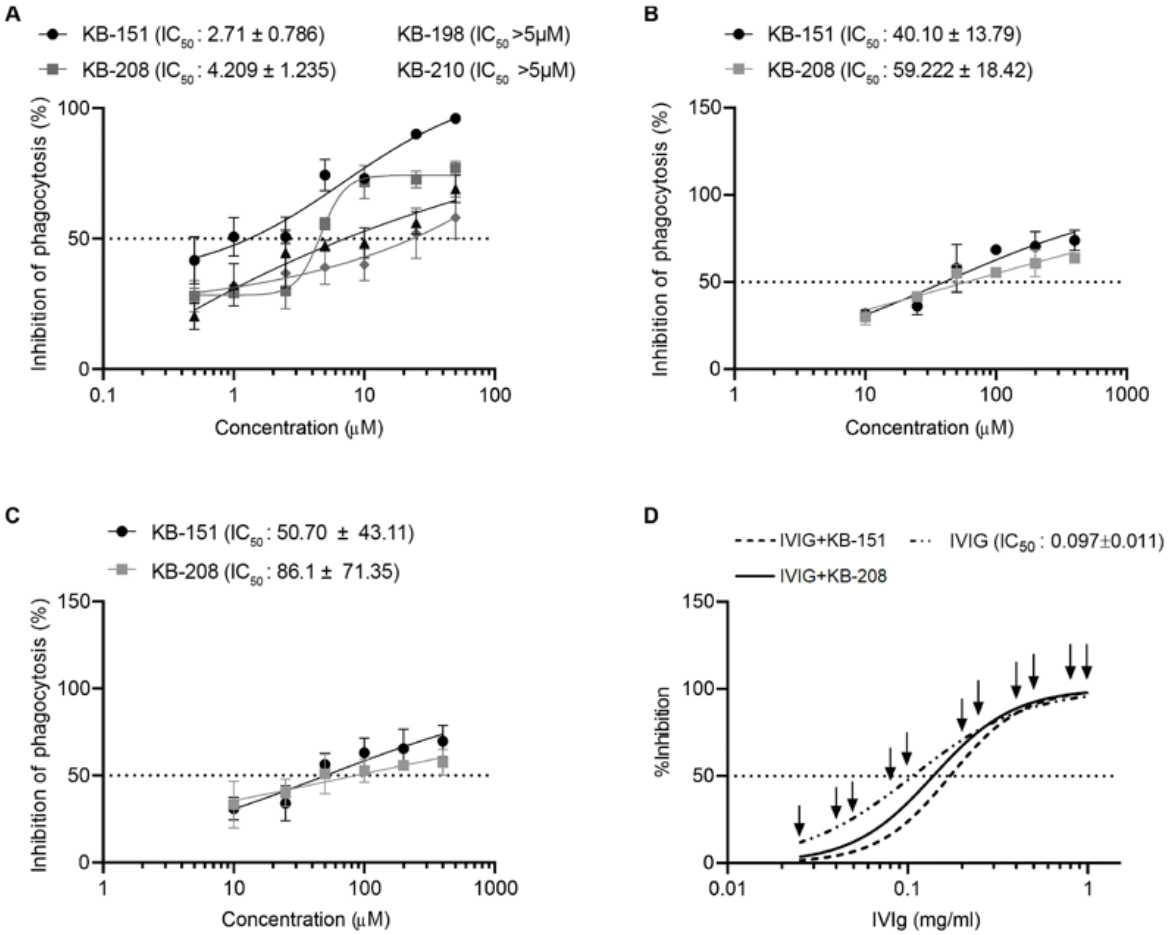


Figure 5. (**A**) Human PBMC's IC_{50}s for the top four compounds. (**B**) Mouse PBMC's IC_{50}s for the two lead compounds. (**C**) Mouse macrophages, RAW 264.7's, IC_{50}s for the two lead compounds. (**D**) Dose-inhibitory response of IVIG alone (IC_{50} = 0.097 ± 0.011) or with addition of **KB-208** (___) or **KB-151** (—-) at their IC_{50} (hPBMCs) concentrations (4μM and 3μM, respectively). Lead compounds are administered along with IVIG at each IVIG concentration used in its titration (arrows). Bars represent mean ± SD, and N = 3.

The cooperation of lead compounds **KB-151** and **KB-208** with IVIG in a dose-inhibitory assay were also evaluated. IVIG was titrated alone and in combination with each test compound (IVIG + test compound), at each IVIG concentration using their IC_{50} concentrations (**KB-151**, 3 μM and **KB-208**, 4 μM). Shifting of the IVIG titration curve would indicate cooperation (synergy) with the KB compound(s), however, the compounds had no effect on the IVIG dose-response curve (Figure 5D).

2.5. Additional Toxicity Testing

Further toxicity studies were conducted using higher concentrations of each lead compound **KB-151** and **KB-208**—up to 250 μM—in LDH, MTT, and apoptosis assays (Annexin V/PI). Figure 6 shows MTT and LDH results for PBMC, Hep G2, and HEK-293 using high concentration (up to 250 μM) of **KB-151** (Figure 6A) and **KB-208** (Figure 6B). Similar experiments with PBMCs incubated with different concentration of **KB-151** and **KB-208** for 24 h were also performed (Figure 7). All compounds showed low to no toxicity using peripheral blood mononuclear cells (PBMCs), liver Hep G2, and kidney HEK293 cell. No significant difference was found between cells treated with leading compound and untreated control. PBMCs showed more than 90% metabolic activity up to 100 μM and less than 11% LDH released in culture media at 250 μM after 24 h incubations.

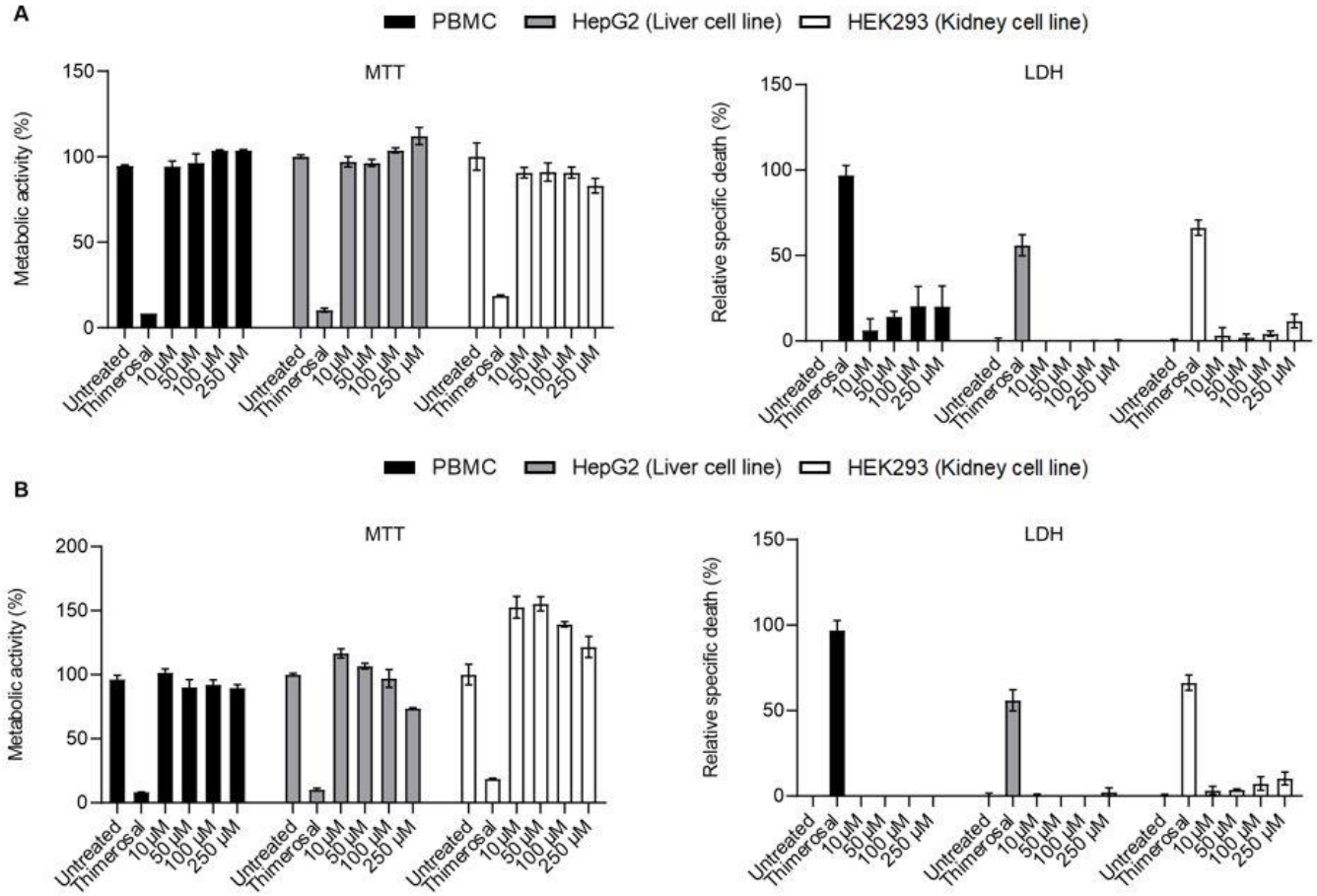


Figure 6. MTT (**left**) and LDH (**right**) results for PBMC (Black), Hep G2 (Grey), and HEK-293 (White) using high concentration (up to 250 µM) of **KB-151** (**A**) and **KB-208** (**B**). *Y*-axis for MTT graph shows the percentage of metabolic activity which is related to the cell viability, and for LDH graph, it shows the percentage of relative specific death which related to the cell toxicity. *X*-axis of both MT and LDH show different concentrations of **KB-151** and **KB-208**, Thimerosal at 100 µM as control toxicity (**** $p \leq 0.0001$), and untreated control. Bars represent mean ± SD, and N = 3.

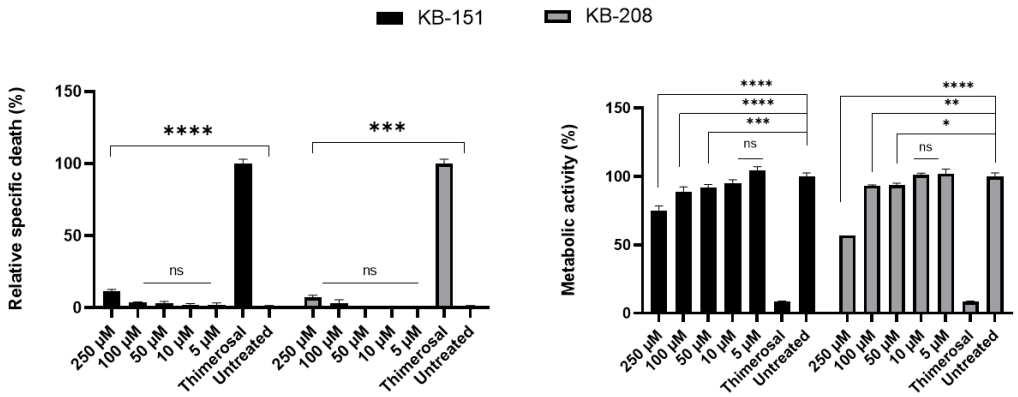


Figure 7. Toxicity assay after 24 h incubation of PBMCs with **KB-151** and **KB-208**. MTT (**right**) and LDH (**left**) results for PBMC using high concentration (up to 250 µM) of **KB-151** (black) and **KB-208** (grey). *Y*-axis for MTT graph shows the percentage of metabolic activity which is related to the cell viability and for LDH graph, shows the percentage of relative specific death which related to the cell toxicity. *X*-axis of both MTT and LDH show different concentrations of **KB-151** and **KB-208**, Thimerosal at 100 µM as control toxicity (* $p < 0.05$, ** $p < 0.01$, *** $p < 0.001$ and **** $p < 0.0001$), and untreated control. Bars represent mean ± SD, and N = 3.

2.6. Apoptosis Assays

Apoptosis assay results for PBMC, Hep G2, and HEK-293 are represented in Figure 8. **KB-151** and **KB-208** showed the same patterns in PBMC, Hep G2, HEK-293, and were similar to untreated cells (Figure 8A). They also showed no significant changes in % viability compared to untreated control in the different cell types (Figure 8B). Similar experiments with PBMCs incubated with different concentrations of **KB-151** and **KB-208** for 24 h were also performed (Figure 8C). In the apoptosis assay, only 70% of the cells were viable, in comparison to 60% for MTT and >89% by LDH.

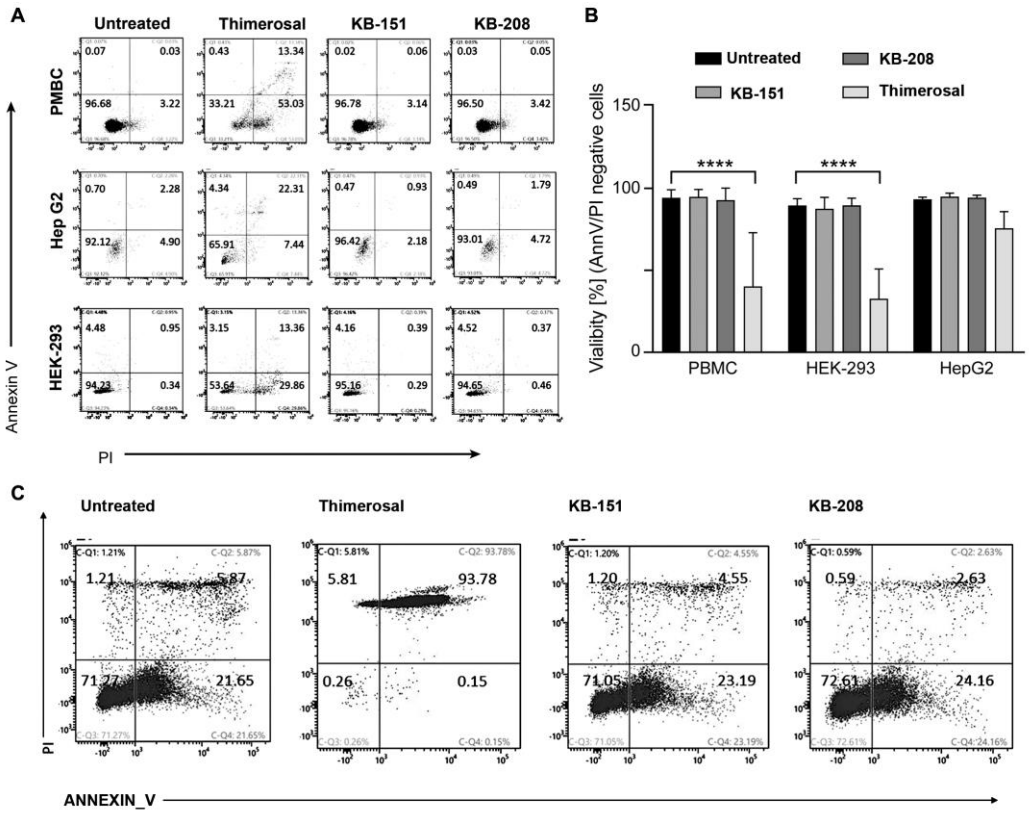


Figure 8. Apoptosis assay for PBMC, Hep G2, and HEK-293 all treated with **KB-151** and **KB-208** at 250 μM concentration for 1 h. (**A**) Representative example of treatments (**B**) Summary of three independent experiments (**** $p < 0.0001$). (**C**) PBMC treated with **KB-151** and **KB-208** at 250 μM concentration for 24 h.

3. Discussion

There are few proven treatments for severe cases of immune cytopenia. Most novel therapies have targeted ITP over other variants of immune cytopenias, such as AIHA, HTR, DHTR, or HDFN. Prevalent therapies include corticosteroids (dexamethasone, prednisone) and rituximab (anti-CD20), as well as IVIG and anti-D [14–16]. There are various alternatives to the use of IVIG in ITP, including thrombopoietin receptor agonists (TPOS-Ras; Eltrombopag and Avatrombopag), anti-D, spleen tyrosine kinase (Syk) inhibitors (fostamatinib), and splenectomy [17–20]. However, since current therapies requires time to be effective, they cannot be used in acute ITP, HTR, DHTR, or HDFN and fulminant AIHA, where the patient may rapidly hemolyze to death. As a result, treatments that can rapidly reverse the immune-mediated destruction of specific blood cells would be highly beneficial. More specifically, they would provide additional time for implementing other therapeutic strategies leading to a higher chance of patient survival.

To date, only small molecules have been developed to treat ITP, such as the orally administered Syk inhibitor Fostamatinib, for patients with chronic ITP who are unresponsive to other treatment options [17,18]. This latest ATP-competitive prodrug is rapidly

dephosphorylated to its active metabolite R-406 in the stomach and acts by blocking Fc-activating receptors. Syk-inhibitors are not specific for monocyte-macrophage Fc receptors, but also target critical signaling pathways in B-cells and T-cells. Other FDA-approved small molecules currently used in the treatment of ITP include the orally administered TPO-RAs Eltrombopag and Avatrombopag [19]. Although their mechanism of action involves stimulation of the TPO receptor on megakaryocytes and hematopoietic pluripotent stem cells, these TPO-RAs are efficacious because they promote platelet precursor survival and increase platelet production by reversing the low platelet production in the bone marrow. Unfortunately, treatments with current small molecules are limited to chronic ITP patients and may require long-term use. Hence, developing small molecules that would be more specific, orally bioavailable, and have a broader application is a worthwhile endeavour. These inhibitors could be administered as sole therapeutics or co-administered with other ITP treatment options. Interest in drug discovery to identify small molecule phagocytosis inhibitors led to our initial publication showing compounds with a disulfide bond (S-S) as in vitro inhibitors of phagocytosis [5]. Since reactive groups such S-S are undesirable in good druggable compounds, additional focused libraries based on 2nd generation phenyl pyrazoles and with desirable chemical structures were synthesized [5]. An iterative exploration of 3rd generation structures incorporating pyrazoles, isoxazoles (for solubility improvement), and pyrroles linked to various heterocycles via alkyl groups (for favourable interactions with the reactive portions in the cell surface of the macrophage) (unpublished results; Figure S1 Supplementary Material) was also conducted. These modified structures were less superior at blocking in vitro phagocytosis, with % inhibition less than 40% (unpublished results). Attempts were made to build computational models using 2D quantitative structure-activity relationship (2D QDSAR), but reliable models could not be obtained.

As reported herein, a focused effort involving in silico screening of a commercial library of over 13,000 compounds was conducted, and a subset of 5000 compounds was obtained. The compounds in the subset were chosen using criteria such as the number of chiral centers (less than 4) and no natural products. Additionally, since one of the goals of this research is to subsequently move to in vivo testing in animal models of immune cytopenias, drug-like properties such as cLogP (no greater than 4), heteroatoms (greater than 3), and molecular weight (200–500 Da) were also considered. This library was further filtered for compounds with similar structural characteristics of previous efficacious small molecules, such as substituted phenyl pyrazole or pyrrole, or the structural features of KB-57—an active compound reported in our previous publication [5] with some in vivo activity. From this filter, a focused library of 80 diverse compounds, with predictable solubility and small molecule drug-like characteristics, was obtained (Figures 1 and 2). Of the 80 compounds evaluated, **KB-151** and **KB-208** significantly inhibited phagocytosis in human monocyte-macrophages, at low μM IC_{50} concentrations. The use of 10 donors in the phagocytosis assays of each hit compound allowed for better determination of mean IC_{50} (±SD) values. Inevitably, the donor-to-donor variability subsequently led to variability in the observed IC_{50} values. Nevertheless, the observed IC_{50} values are considered low and relatively reproducible.

Both lead compounds **KB-151** and **KB-208** exhibited minimal to no toxicity in vitro up to 250 μM (highest concentration tested) at 1 h, but after 24 h at 250 μM, toxicity was observed. These toxicity results are promising and should pose no concerns, since the compounds would likely not be administered at such high doses once moved to in vivo experiments.

KB-151 and **KB-208** were also able to inhibit phagocytosis in a murine system, albeit at a higher IC_{50} values. There are considerable differences between human and mouse monocyte-macrophages [21], therefore, the observed differences in IC_{50} values were not surprising. However, these IC_{50} values in mouse monocytes and macrophages indicate the starting doses of these compounds that should be used when they are evaluated in vivo, in the mouse model of ITP.

The pyrazole-containing compounds described herein show promise as potential small molecule inhibitors of phagocytosis. However, improved efficacy of these compounds, including the hit molecules, needs to be investigated in SAR studies, through modification or elimination of functional groups on the pyrazole core moiety. Future in vivo evaluation of these lead compounds may include (i) efficacy to ameliorate experimental ITP and AIHA; (ii) optimal administration route (IP, IV, subcutaneous, peroral) and (iii) dosing, with and without low-dose IVIG (for synergy). The lead candidate(s) that shows efficacy to reverse ITP and/or AIHA, or cooperate with IVIG to increase efficacy, may be tested for toxicity by pathological exams, histology, and immunohistochemistry of multiple organs. Likewise, further experiments are needed to determine the mechanism of action, since the possibility exists for blockade of Fc receptor proteins by these small molecules. Still, this effect is difficult to prove and, alternatively, they may affect signaling pathways. Additionally, the pharmacokinetics of the efficacious molecules, as well as the biodistribution of the molecules once administered, may be examined.

4. Materials and Methods

4.1. Selection of Compounds for Preliminary In Vitro Screening

From a commercial library of over 13,000 compounds, an in silico screen was conducted using physicochemical parameters, such as the number of chiral centers, heteroatoms, molecular weight and cLogP values. From these results, a 5000 compound library was acquired in the form of 10 mM DMSO solutions. Using several core structural moieties of previously investigated small molecules, this 5000 compound library was further narrowed to 80 compounds for preliminary in vitro iterative exploration.

The structures and purity for all 5000 compounds, including the final 80 selected and tested compounds, were recorded using ^{1}H-NMR spectroscopy and/or HPLC-ELSD-DAD-MS. These data were supplied by the chemical library vendor and verified by us. All compounds are at least 95% pure, as confirmed by the chemical library vendor.

The four hit compounds (KB-151, KB-198, KB-208, and KB-210) were further analyzed in our laboratories using ^{1}H-NMR, HPLC-PDA-MS, and UHPLC-HRMS/MS, and their purities were re-evaluated.

4.2. Characterization by ^{1}H-NMR

^{1}H-NMR experiments were recorded on a Bruker Avance 400 MHz spectrometer and chemical shifts are reported in δ ppm using $CDCl_3$ (with tetramethylsilane as the internal standard) (Supplementary Data Figures S3–S6).

4.3. Characterization by UHPLC-HRMS/MS

The UHPLC-HRMS/MS profiles of the compounds (Supplementary Data Figures S7–S10) were obtained by a tandem LC-MS/MS system. UHPLC was performed on a Thermo Scientific Ultimate 3000 UHPLC system with a Thermo Scientific Hypersil Gold C_{18} column (50 mm × 2.1 mm, 1.9 µm I.D.) equipped with guard column. The mobile phase for UHPLC analysis consisted of water (A) and acetonitrile (B), each with 0.1% formic acid. The sample injection plate and the column were maintained at 5 °C and 40 °C, respectively. The gradient was programmed as follows: 0–0.5 min (50% A/50% B), 0.5–2 min (50% A/50% B to 0% A/100% B, gradient), 2–10 min (0% A/100% B), 10–10.5 min (0% A/100% B to 50% A/50% B, gradient), and 10.5–15 min (50% A/50% B). The flow-rate was 0.4 mL/min.

HRMS/MS was performed on a Thermo Scientific Q Exactive mass spectrometer equipped with a HESI-II probe. MS data were acquired in positive polarity, and the full MS (MS1) data (300–500 Da; resolution = 140,000) and parallel reaction monitoring (MS2) data (resolution = 17,500) were collected.

4.4. % Purity and Characterization by PDA

The purity of the compounds (two solvent systems; Supplementary Data Table S1 and Figures S11–S17) was determined by tandem HPLC-PDA-MS equipped with a Waters®

2545 binary gradient module, Waters® PDA 2998 photodiode array detector (190–800 nm) and a Waters® QDa mass spectrometer (200–1200 Da). HPLC was performed on an X-Bridge® analytical C_{18} column (4.6 mm × 150 mm, 5 µm I.D.). Mass spectra were recorded using ESI (+ve) mode (200–800 Da). All HPLC solvents are HPLC grade. The purity methods used for analysis are as follows:

Method A: The mobile phase for HPLC-PDA-MS analysis consisted of water (A) and methanol (B), each with 0.1% formic acid. The gradient was programmed as follows: 0–9 min (50% A/50% B to 2% A/98% B, gradient), 9–10 min (2% A/98%B); 10–11 min (2% A/98% B to 50% A/50%B, gradient), and 11–15 min (50% A/50%B). The flow-rate was 1 mL/min.

Method B: The mobile phase for analysis consisted of water (A) and acetonitrile (B), each with 0.1% formic acid. The gradient was programmed as follows: 0–9 min (50% A/50% B to 2%A/98% B, gradient), 9–10 min (2% A/98%B); 10–11 min (2% A/98% B to 50% A/50%B, gradient), and 11–15 min (50% A/50%B). The flow-rate was 1 mL/min.

4.5. Spectroscopic Data

KB-151: ^{1}H-NMR ($CDCl_3$, 400 MHz) δ ppm: 10.42 (s, 2H, H6), 7.73–7.70 (m, 2H, H1), 7.57–7.48 (m, 4H, H2 & H3), 4.52 (q, *J* = 7.3 Hz, 2H, H4), 4.26 (q, *J* = 7.5 Hz, 2H, H8), 1.57 (t, 3H, H5), 1.47 (t, 3H, H9); HRMS (HESI) *m/z*: $[M+H]^+$ Calcd for $C_{19}H_{18}BrN_6O_3$ 457.0618; found 457.0623.

KB-198: ^{1}H-NMR ($CDCl_3$, 400 MHz) δ ppm: 7.50 (s, 1H, H13), 7.22 (d, *J* = 2.0 Hz, 2H, H3), 6.95 (s, 1H, H10), 5.90 (d, 1H, H4), 5.07 (d, *J* = 4.2, 7.8 Hz, 1H, H5), 4.19–4.02 (m, 2H, H2), 3.64 (dt, *J* = 7.2, 10 Hz, 1H. H8′), 3.44–3.39 (m, 1H, H8″), 2.42 (s, 3H, H9), 2.35–2.26 (m, 1H, H6′), 2.21 (s, 3H, H12), 2.18 (s, 3H, H11), 2.12–1.95 (m, 2H, H6″ & H7′), 1.92–1.85 (m, 1H, H7″), 1.38 (t, 3H, H1); HRMS (HESI) *m/z*: $[M+H]^+$ Calcd for $C_{18}H_{26}N_3O_2S$ 348.1740; found 348.1739.

KB-208: ^{1}H-NMR ($CDCl_3$, 400 MHz) δ ppm: 7.43–7.35 (m, 5H, H1, H2 & H3), 7.29 (d, *J* = 4.8 Hz, 1H, H4), 7.95 (dd, *J* = 3.7, 5.0 Hz, 1H, H5), 6.91 (s, 1H, H7), 6.84 (d, 1H, H6), 4.77 (t, *J* = 15.3 Hz, 2H, H8′), 3.67 (s, 3H, H12), 3.17 (t, *J* = 13.9 Hz, 1H, $H8^{a''}$), 2.80 (t, 1H, $H8^{b''}$), 2.27 (dd, *J* = 2.6, 7.5 Hz, 2H, H11), 2.15–2.06 (m, 1H, H10), 1.81 (dd, *J* = 14.1, 25.0 Hz, 2H, H9′), 1.37–1.24 (m, 2H, H9″); HRMS (HESI) *m/z*: $[M+H]^+$ Calcd for $C_{22}H_{24}N_3O_3S$ 410.1533; found 410.1531.

KB-210: ^{1}H-NMR ($CDCl_3$, 400 MHz) δ ppm: 8.33 (s, 1H, H4), 7.40 (d, *J* = 3.5 Hz, 1H, H8), 7.38–7.34 (m, 3H, H1 & H2′), 7.20–7.15 (m, 2H, H2″ & H3), 6.96 (d, 1H, H6, H7), 6.83–6.82 (m, 2H, H5), 6.53–6.52 (m, 2H, H6); HRMS (HESI) *m/z*: $[M+H]^+$ Calcd for $C_{17}H_{14}N_5OS$ 336.0914; found 336.0912.

4.6. Primary Cells and Cell Lines

Upon informed consent, blood from healthy volunteers was collected in ac-id-citrate-dextrose (ACD) anticoagulant-containing tubes. Mononuclear cells (PBMC) were obtained by density centrifugation using Ficoll–Hypaque solution (Biochrom AG, Berlin Germany). Primary monocytes for functional phagocytosis assays were separated as described below.

All cell lines were purchased from American Type Culture Collection (ATCC, Manassas, VA, USA) and were tested free for mycoplasma. The cell lines used include: human 293[HEK-293, cat #CFL-1573, a human kidney embryo-derived cell line (kidney); human Hep G2[HEPG2, cat #HB-8065, a human-derived hepatocellular carcincoma cell line (liver); and LRRK2 parental RAW 264.7[RAW 264.7] mouse macrophages, cat #SC-6003. Hep G2 and HEK293 cell lines were cultured in Eagle's Minimum Essential Medium (EMEM) supplemented with 10% fetal bovine serum, whereas RAW 264.7 cell lines were cultured in Dulbecco's Modified Eagle Medium (DMEM) supplemented with 10% fetal bovine serum.

4.7. Phagocytosis Assay

The MMA to screen compounds for their ability to inhibit phagocytosis was performed as previously described [14,15]. Briefly, PBMCs were layered onto chamber slides and

monocytes purified by adherence after 1 hr at 37 °C with 5% CO_2. Drugs were solubilized in 100% DMSO and then diluted in RPMI to the final concentration of 5 μM, as previously reported [7]. Corresponding DMSO volumes in RPMI were used as a control. Final DMSO concentration used was $\leq$1% v/v. After 1 hr, indicator Rh-positive red cells opsonized with anti-RhD were added to the chamber slides and then further incubated for 2 hrs before fixing and counting phagocytosed RBCs using phase-contrast microscopy [7]. As a positive control for inhibition, IVIG, known to inhibit phagocytosis due to blocking of FcγRs, was used [7]. The phagocytosis index (PI) was determined as the number of phagocytosed RBCs in 100 monocytes. The percent inhibition of phagocytosis was determined by comparing the PI in each treated sample to the PI in the untreated sample, which was determined by normalizing the PI concentration in each treated sample (phagocytosis of opsonized RBCs with vehicle only, representing 100 percent phagocytosis).

$$\text{PI} = \frac{\text{\# of phagocytic RBCs}}{\text{300 monocytes}} \times 100 \quad (1)$$

4.8. Cell Viability Assays

MTT Assay. The MTT assay was used to assess the impact of the selected compounds on the metabolic activity of primary mononuclear cells [12,13]. PBMCs (5 × 104 total cells per well) were isolated from ACD tubes and seeded on 96 culture plates (VWR® Tissue Culture Plate, Untreated, Sterilized, Non-Pyrogenic). Cells were treated with 5 μM of the solubilized compounds and incubated for three hours at 37 °C with 5% CO_2. After that, MTT was added to the cells and plates were incubated for 2 hrs. The formation of formazan purple crystals was followed under a light microscope. We solubilized the formazan crystals by incubating overnight with 100 μL of 10% SDS, 0.01M HCl SDS. Absorbance was measured at 570 (reference 690 nm) in a BioTek EPOCH 2 microplate reader with Gen 5 Ver. 2.05 software (BioTek, Winooski, VT, USA). As a positive control for decreased metabolic activity, 100 μM thimerosal (diluted in RPMI) was used. Untreated cells represented the basal metabolic activity of the cells. This experiment is repeated at increasing concentrations (250 μM, 100 μM, 50 μM, and 10 μM) for the two lead compounds (KB-151 and KB-208) using a variety of cell types, including PBMC, Hep G2, and HEK-293.

LDH Assay. To understand if any of the studied compounds induced primary cell death (PBMC), LDH release was evaluated as a measure of cytotoxicity [10]. To this end, an LDH-cytotoxicity test kit (Sigma Inc., Marlborough, MA, USA) was used according to the manufacturer's instructions. Sample treatment was performed identically to the MTT assay previously described. The absorbance at 490 and 600 nm was determined using a microplate reader (Bio-Rad EPOCH II). Minimum lysis control is referred to as samples without treatment. Cells solubilized with a lysis buffer provided with the kit are considered as maximum lysis control. Specific cell death was calculated as:

$$\%\ \text{Specific Death} = \frac{(\text{Experimental Lysis} - \text{Minimum Lysis})}{(\text{Maximum Lysis} - \text{Minimum Lysis})} \times 100 \quad (2)$$

This experiment was repeated at increasing concentrations (250 μM, 100 μM, 50 μM, and 10 μM) for the two lead compounds (**KB-151** and **KB-208**) using a variety of cell types, including PBMC, Hep G2, and HEK-293.

4.9. Apoptosis Assay

PBMC, Hep G2, and HEK-293 cells were treated for 1 hr with KB-151 and **KB-208** at a 250 μM concentration. Thimerosal (100 μM) was utilized as a positive control for viability (diluted in RPMI). Staining with Annexin V and PI was performed according to the manufacturer's procedure for the Annexin-V-FLUOS Staining Kit (Sigma), and samples were run through an SP6800 Spectral Cytometer.

4.10. Dose-Inhibitory Response and IC_{50}

MMAs (as explained in detail in Section 4.7) were repeated with different concentration of four hit compounds (**KB-151**, **KB-198**, **KB-208**, and **KB-210**), including 100 µM, 50 µM, 25 µM, 10 µM, 5 µM, 2.5 µM, 1 µM, and 0.5 µM with human PBMCs. Dose-inhibitory response experiments were also repeated for RAW 264.7 and mouse (BA:B/c) PBMCs with different concentrations of two lead compounds (**KB-151** and **KB-208**), including 400 µM, 200 µM, 100 µM, 50 µM, 25 µM, and 10µM.

Supplementary Materials: The following supporting information can be downloaded at: https://www.mdpi.com/article/10.3390/molecules28020757/s1, Figure S1: Unpublished 3rd generation structures based on merging the features of **KB-55**, **KB-57,** and **KB-59** [6]; Figure S2: ^{1}H-NMR spectrum of **KB-151** in $CDCl_3$; Figure S3: ^{1}H-NMR spectrum of **KB-198** in $CDCl_3$; Figure S4: ^{1}H-NMR spectrum of **KB-208** in $CDCl_3$; Figure S5: ^{1}H-NMR spectrum of **KB-210** in $CDCl_3$; Figure S6: UHPLC-HRMS/MS data of **KB-151**; Figure S7: UHPLC-HRMS/MS data of **KB-198**; Figure S8: UHPLC-HRMS/MS data of **KB-208**; Figure S9: UHPLC-HRMS/MS data of **KB-210**; Figure S10: HPLC-PDA chromatogram of **KB-151**; Figure S11: HPLC-PDA spectrum of **KB-151**; Figure S12: HPLC-PDA chromatogram of **KB-198**; Figure S13: HPLC-PDA spectrum of **KB-198**; Figure S14: HPLC-PDA chromatogram of **KB-208**; Figure S15: HPLC-PDA spectrum of **KB-208**; Figure S16: HPLC-PDA chromatogram of **KB-210**; Figure S17: HPLC-PDA spectrum of **KB-210**; Table S1: Purity results of hit compounds.

Author Contributions: Conceptualization, L.P.K. and D.R.B.; methodology, M.M.L.-B., L.P.K. and D.R.B.; validation, M.L., M.M.L.-B., K.F.B., S.W. and M.B.H.; formal analysis, M.L., M.M.L.-B., K.F.B., S.W. and M.B.H.; investigation, M.L., M.M.L.-B., K.F.B., S.W. and M.B.H.; resources, L.P.K. and D.R.B.; data curation, M.L. and M.M.L.-B.; writing—original draft preparation, M.L., M.M.L.-B., L.P.K. and D.R.B.; writing—review and editing, M.L., M.M.L.-B., L.P.K. and D.R.B.; visualization, M.M.L.-B., L.P.K. and D.R.B.; supervision, L.P.K. and D.R.B.; project administration, L.P.K. and D.R.B.; funding acquisition, L.P.K. and D.R.B. All authors have read and agreed to the published version of the manuscript.

Funding: This research was funded by the Canadian Blood Services (CBS) Intramural Funding Program, grant number XT00136.

Institutional Review Board Statement: Not applicable.

Informed Consent Statement: Not applicable.

Data Availability Statement: Not applicable.

Acknowledgments: M.L. is a recipient of a CBS Graduate Fellowship Program (GFP) award. K.F.B. is a recipient of a CBS Postdoctoral Fellowship (PDF) award.

Conflicts of Interest: The authors declare no conflict of interest.

References

1. Gilliland, B.C.; Evans, R.S. The immune cytopenias. *Postgrad. Med.* **1973**, *54*, 195–203. [CrossRef] [PubMed]
2. Petz, L.D.; Garratty, G. *Immune Hemolytic Anemias*, 2nd ed.; Petz, L.D., Garratty, G., Eds.; Churchill Livingstone: Philadelphia, PA, USA, 2004. [CrossRef]
3. Connell, N.T.; Berliner, N. Fostamatinib for the treatment of chronic immune thrombocytopenia. *Blood* **2019**, *133*, 2027–2030. [CrossRef]
4. Zuercher, A.W.; Spirig, R.; Baz Morelli, A.; Rowe, T.; Käsermann, F. Next generation Fc receptor-targeting biologics for autoimmune diseases. *Autoimmun. Rev.* **2019**, *18*, 102366. [CrossRef]
5. Purohit, M.K.; Scovell, I.; Neschadim, A.; Katsman, Y.; Branch, D.R.; Kotra, L.P. Disulfide linked pyrazole derivatives inhibit phagocytosis of opsonized blood cells. *Bioorg. Med. Chem. Lett.* **2013**, *23*, 2324–2327. [CrossRef] [PubMed]
6. Purohit, M.K.; Chakka, S.K.; Scovell, I.; Neschadim, A.; Bello, A.M.; Salum, N.; Katsman, Y.; Bareau, M.C.; Branch, D.R.; Kotra, L.P. Structure-activity relationships of pyrazole derivatives as potential therapeutics for immune thrombocytopenias. *Bioorg. Med. Chem.* **2014**, *22*, 2739–2752. [CrossRef] [PubMed]
7. Tong, T.N.; Branch, D.R. Use of a Monocyte Monolayer Assay to Evaluate Fcγ Receptor-mediated Phagocytosis. *J. Vis. Exp.* **2017**, *119*, 55039. [CrossRef]
8. Tong, T.N.; Cen, S.; Branch, D.R. The Monocyte Monolayer Assay: Past, Present and Future. *Transfus. Med. Rev.* **2019**, *33*, 24–28. [CrossRef] [PubMed]

9. Nance, S.J.; Arndt, P.; Garratty, G. Predicting the clinical significance of red cell alloantibodies using a monocyte monolayer assay. *Transfusion* **1987**, *27*, 449–452. [CrossRef] [PubMed]
10. Kumar, P.; Nagarajan, A.; Uchil, P.D. Analysis of Cell Viability by the Lactate Dehydrogenase Assay. *Cold Spring Harb. Protoc.* **2018**, *2018*, pdb-prot095497. [CrossRef] [PubMed]
11. Rampersad, G.C.; Suck, G.; Sakac, D.; Fahim, S.; Foo, A.; Denomme, G.A.; Langler, R.F.; Branch, D.R. Chemical compounds that target thiol-disulfide groups on mononuclear phagocytes inhibit immune mediated phagocytosis of red blood cells. *Transfusion* **2005**, *45*, 384–393. [CrossRef] [PubMed]
12. Branch, D.R.; Guilbert, L.J. Practical in vitro assay systems for the measurement of hematopoietic growth factors. *J. Tissue Cult. Methods* **1986**, *10*, 101–107. [CrossRef]
13. Berridge, M.V.; Tan, A.S. Characterization of the cellular reduction of 3-(4,5-dimethylthiazol-2-yl)-2,5-diphenyltetrazolium bromide (MTT): Subcellular localization, substrate dependence, and involvement of mitochondrial electron transport in MTT reduction. *Arch. Biochem. Biophys.* **1993**, *303*, 474–482. [CrossRef] [PubMed]
14. Ghanima, W.; Godeau, B.; Cines, D.B.; Bussel, J.B. How I treat immune thrombocytopenia: The choice between splenectomy or a medical therapy as a second-line treatment. *Blood* **2012**, *120*, 960–969. [CrossRef] [PubMed]
15. Thompson, J.C.; Klima, J.; Despotovic, J.M.; O'Brien, S.H. Anti-D immunoglobulin therapy for pediatric ITP: Before and after the FDA's black box warning. *Pediatr. Blood Cancer* **2013**, *60*, E149–E151. [CrossRef] [PubMed]
16. Long, M.; Kalish, L.A.; Neufeld, E.J.; Grace, R.F. Trends in anti-D immune globulin for childhood immune thrombocytopenia: Usage, response rates, and adverse effects. *Am. J. Hematol.* **2012**, *87*, 315–317. [CrossRef] [PubMed]
17. Braselmann, S.; Taylor, V.; Zhao, H.; Wang, S.; Sylvain, C.; Baluom, M.; Qu, K.; Herlaar, E.; Lau, A.; Young, C.; et al. R406, an orally available spleen tyrosine kinase inhibitor blocks fc receptor signaling and reduces immune complex-mediated inflammation. *J. Pharmacol. Exp. Ther.* **2006**, *319*, 998–1008. [CrossRef] [PubMed]
18. McKeage, K.; Lyseng-Williamson, K.A. Fostamatinib in chronic immune thrombocytopenia: A profile of its use in the USA. *Drugs Ther. Perspect.* **2018**, *34*, 451–456. [CrossRef] [PubMed]
19. Cheloff, A.Z.; Al-Samkari, H. Avatrombopag for the treatment of immune thrombocytopenia and thrombocytopenia of chronic liver disease. *J. Blood Med.* **2019**, *10*, 313–321. [CrossRef] [PubMed]
20. Cohn, C.S.; Bussel, J.B. Romiplostim: A second-generation thrombopoietin agonist. *Drugs Today* **2009**, *45*, 175–188. [CrossRef] [PubMed]
21. Ingersoll, M.A.; Spanbroek, R.; Lottaz, C.; Gautier, E.L.; Frankenberger, M.; Hoffmann, R.; Lang, R.; Haniffa, M.; Collin, M.; Tacke, F.; et al. Comparison of gene expression profiles between human and mouse monocyte subsets. *Blood* **2010**, *115*, e10–e19. [CrossRef] [PubMed]

Disclaimer/Publisher's Note: The statements, opinions and data contained in all publications are solely those of the individual author(s) and contributor(s) and not of MDPI and/or the editor(s). MDPI and/or the editor(s) disclaim responsibility for any injury to people or property resulting from any ideas, methods, instructions or products referred to in the content.